Astron. Astrophys. 336, 103–115 (1998)

ASTRONOMY AND ASTROPHYSICS

# On the oxygen abundance deficiency in spiral galaxies

**L.S. Pilyugin**[1] **and F. Ferrini**[2]

[1] Main Astronomical Observatory of National Academy of Sciences of Ukraine, Goloseevo, 252650 Kiev-22, Ukraine (pilyugin@mao.kiev.ua)
[2] Department of Physics, Section of Astronomy, University of Pisa, Piazza Torricelli 2, I-56100 Pisa, Italy (federico@astr2pi.difi.unipi.it)

Received 10 March 1998 / Accepted 12 May 1998

**Abstract.** The observed radial distributions of oxygen abundance in twelve spiral galaxies of various Hubble types from Sab to Sd have been compared with predictions of the closed-box model for chemical and photometric evolution of galaxies, with the purpose of searching for the deficiency of oxygen abundance in galaxies: this is an indicator of gas exchange between galaxy and its environments or/and redistribution of gas (heavy elements) within disk.

It has been found that among high luminosity spiral galaxies, only NGC3031 (M81) – a well known interacting galaxy – has a large oxygen abundance deficiency. Other high luminosity galaxies have no, or have a moderate deficiency of oxygen abundance.

All the low luminosity Scd and Sd galaxies show a significant deficiency of oxygen abundance. This can be considered as an evidence in favor of that these galaxies lost a part of the heavy elements content in the course of their evolution. By considering the definition of late-type giant galaxies versus late-type dwarf galaxies dichotomy by Binggeli: "dwarf galaxies did, classical (giant) galaxies did not, suffer global mass loss by galactic winds", the present result leads to the conclusion that the transition from late-type giants to late-type dwarfs occurs within the class Scd.

**Key words:** galaxies: abundances – galaxies: evolution - galaxies: ISM – galaxies: spiral

## 1. Introduction

The detailed study of the structure and evolution of galaxies is becoming feasible thanks to the large increase of observations that has been recently accumulated. The analysis of the heavy elements abundance history and of its relationship with other large scale galactic properties are based on a reasonable experimental basis. In investigations of the relationship between the oxygen abundance and the macroscopic properties of spiral galaxies, the concept of the characteristic oxygen abundance has been introduced: it is defined as the oxygen abundance at a predetermined galactocentric distance $r^*$. Due to the presence of radial abundance gradients in the disks of spiral galaxies, the choice of the "representative" value of oxygen abundance in a galaxy is not a trivial matter. The extrapolated central intersect abundance ($r^* = 0$), the oxygen abundance at $r^* = 0.4\rho_0$, where $\rho_0$ is the isophotal radius (the radius at which the surface brightness equals 25.0 mag arcsec$^{-2}$), and the oxygen abundance at $r^* = \rho_S$, where $\rho_S$ is the the disk scale length, have been used as the characteristic oxygen abundance in the galaxy (Vila-Costas & Edmunds 1992; Zaritsky, Kennicutt & Huchra 1994, ZKH; Garnett et al 1997). With any choice of $r^*$, the value of $O/H(r^*)$ is a local parameter, i.e. represents the oxygen abundance in the region at a given galactocentric distance but not the oxygen abundance of the whole galaxy.

Several reasons are responsible for the oxygen abundance present at a given galactocentric distance. First, its value depends on the evolutionary stage of the region, i.e. on the astration level or gas mass fraction in the region. Second, the local oxygen abundance depends on the gas exchange between galaxy and its environments (unenriched gas infall onto the galaxy or/and gas loss via galactic winds). Third, the local oxygen abundance depends on the gas exchange between the chosen region and other regions of the galaxy (radial gas flows or gas exchange between different rings of the disk through halo via galactic fountain), i.e. the local oxygen abundance depends on the redistribution of gas (hea vy elements) within disk. Hence, we may conclude that the value of the characteristic oxygen abundance in the galaxy depends on i) the arbitrary choice of $r^*$, ii) the evolutionary stage of the chosen region, iii) the mass exchanges between the chosen region and its environment. Therefore, different reasons can be responsible for the variations of the characteristic oxygen abundance among galaxies.

In the present study, the concept of the oxygen abundance deficiency in the galaxy is introduced as a deficiency of the oxygen abundance observed in the galaxy in comparison to the oxygen abundance predicted by the closed-box model for the same gas mass fraction. There are two significant advantages by choosing the oxygen abundance deficiency in the galaxy instead of the characteristic oxygen abundance. First, its value is independent of the evolutionary stage of the galaxy. Second, the value of the oxygen abundance deficiency can be derived for the whole disk (value of global oxygen abundance deficiency) as well as for a particular region (value of local oxygen abundance

*Send offprint requests to*: L.S. Pilyugin

deficiency). The variations of the value of oxygen abundance deficiency from region to region of a galaxy or from galaxy to galaxy can be only caused by the variations of efficiency of gas exchange between galaxies (regions) and their environments (it should be noted that in the case of chosen region of the disk, other regions of the disk are environments). In turn, the value of oxygen abundance deficiency can be consid ered as indicative of the efficiency of mass exchange.

In the present study the values of the oxygen abundance deficiency for a number of spiral galaxies will be derived, with the purpose of searching for galaxies with high efficiency of gas exchange with environments. The paper is organized as follows: in Sect. 2 the approach and data base are described: the results are discussed in Sect. 3; Sect. 4 is a brief summary.

## 2. Determination of oxygen abundance deficiency

### *2.1. The approach*

The value of global oxygen abundance deficiency in the disk of a spiral galaxy, $\eta$, is given by the expression:

$$\eta = 1 - \frac{\int_0^{R_G} Z_O^{obs} r\mu(r)\sigma_{tot}(r)dr}{\int_0^{R_G} Z_O^{CB} r\mu(r)\sigma_{tot}(r)dr}, \quad (1)$$

where $Z_O^{obs}(r)$ is the observed oxygen abundance at the radius $r$, $\mu(r)$ is the gas mass fraction in the galaxy at radius $r$, $\sigma_{tot}(r)$ is the total surface mass density, and $Z_O^{CB}(r)$ is the oxygen abundance predicted by the closed-box model for a given value of $\mu(r)$. The parameter $\eta$ gives the deficiency of the oxygen abundance in the gas fraction of the galaxy in comparison to the same quantity deduced from a closed-box model, applied to a galaxy having at present the same gas and total mass distributions.

The excess of oxygen abundance in comparison to the closed-box model of chemical evolution can be caused only by the inflow of over-enriched gas into the galaxy. Since such possibility seems to be unrealistic it can be adopted that the closed-box model gives the upper limit of oxygen abundance in the system with fixed value of gas mass fraction. It should be noted, however, that the gas exchange between different rings of a galaxy can produce an excess of oxygen abundance in a part of the disk, but it can result in no oxygen abundance excess in the whole disk.

To determine the parameter $\eta$, the radial distributions of oxygen abundance $Z_O^{obs}(r)$, of gas mass fraction $\mu(r)$, and of total surface mass density $\sigma_{tot}(r)$ are needed. The gas mass fraction $\mu(r)$ is defined as the ratio of gas mass to the luminous mass:

$$\mu(r) = \sigma_g(r)/(\sigma_g(r) + \sigma_s(r)), \quad (2)$$

where

$$\sigma_g(r) = 1.4(\sigma_{HI}(r) + \sigma_{H_2}(r)), \quad (3)$$

and $\sigma_g(r)$, $\sigma_{HI}(r)$, $\sigma_{H_2}(r)$, $\sigma_s(r)$ are the surface mass density of gas, atomic hydrogen, molecular hydrogen and stars, respectively. The factor of 1.4 is the helium contribution to the mass of interstellar medium.

### *2.2. The data base*

The data base used in this analysis consists of published radial distributions of atomic hydrogen, of molecular hydrogen derived from CO emission, of surface brightness in B or V band, and of oxygen abundance in spiral galaxies. Our list comprises 12 galaxies for which we have collected the relevant observational data. The observational characteristics and literature sources for the observational data of the galaxies in the present sample are summarized in Table 1. The NGC and Messier (if exists) numbers are given in columns 1 and 2, respectively. The adopted distance and corresponding references are listed in columns 3 and 4, respectively. The distances of the Virgo galaxies in our sample (NGC4303 and NGC4321) are equal to the recently measured Cepheid distance of 16.1 Mpc for NGC4321 (Ferrarese et al 1996a, b). The absolute B magnitude as computed from adopted distance and from $B_0^T$ magnitude taken from de Vaucouleurs (1991, RC3) is listed in column 5. The numerical Hubble type of the galaxy (T type, from RC3) is given in column 6. Information on the radial distribution of the surface brightness is reported in columns 7 and 8; the used band is listed in column 7, and the literature sources for radial luminosity profile is reported in column 8. Sources for HI data are listed in column 9. Sources for CO data are given in column 10. Oxygen abundance at center and the value of oxygen abundance gradient are listed in columns 11 and 12, respectively. Finally, the literature source for the oxygen abundance data is reported in column 13.

The radial distribution of the surface mass density of molecular hydrogen has been derived from the observed radial distribution of CO emission. This has been approximated by an exponential law except for NGC224, NGC598, NGC1313, and NGC7793. Since the CO emission measurements exist, as a rule, only for central regions of galaxies, the CO emission in outer regions has been estimated through extrapolation of the exponential law. For NGC224 the table data for CO emission have been used. For NGC598 the exponential fit to the observational data cannot be found, since the CO emission is only mapped out to a $3.'5$ radius and a strong (exponential) decrease in CO emission as a function of radius is not yet seen. The contribution of molecular hydrogen to gas fraction in NGC598 has been taken into account in the central region only. The measurements of CO emission from NGC1313 and from NGC7793 indicate that the amount of molecular hydrogen in these galaxies is small as compared to amount of atomic gas (Harnett et al 1991; Israel et al 1995), and only atomic gas has been taken into account in these galaxies. The CO-to-$H_2$ conversion factor is not beyond question. The CO-to-$H_2$ conversion factor can depend on the metallicity and the ambient radiation field intensity (Wilson 1995, Lequeux 1996, Arimoto et al 1996). In the present study the metallicity-dependent conversion factor from Arimoto et al (1996) has been used

$$X = N_{H_2}/I_{CO} = X^* \times 10^{20}\ \mathrm{cm}^{-2}/(\mathrm{K\ km\ s}^{-1}), \quad (4)$$

where

$$\log X^* = -1.0\,(12 + \log O/H)\ +\ 9.30 \quad (5)$$

**Table 1.** Observational characteristics and literature sources for the observational data of the galaxies in the present sample

| NGC No | other name | d Mpc | ref | $M_B$ | T | band used | ref | sources for HI | sources for CO | 12+logO/H at center | gradient dex/kpc | ref |
|---|---|---|---|---|---|---|---|---|---|---|---|---|
| 1 | 2 | 3 | 4 | 5 | 6 | 7 | 8 | 9 | 10 | 11 | 12 | 13 |
| 224 | M31 | 0.77 | LFM | -21.09 | 3 | B | V,HM,WK | KDIT | KDIT | 9.14 | -0.016 | ZKH |
| 598 | M33 | 0.84 | FWM | -18.88 | 6 | B | V59 | N | WS | 9.08 | -0.106 | ZKH |
| 628 | M74 | 7.26 | SKT | -19.51 | 5 | B | SK | SK | AL | 9.32 | -0.085 | ZKH |
| 1313 | | 4.5 | V63 | -19.00 | 7 | V | Retal | Retal | (Hetal) | 8.56 | -0.003 | WR |
| 2403 | | 3.25 | FM | -19.12 | 6 | B | OTK | WKA | TW | 8.77 | -0.102 | Getal |
| 3031 | M81 | 3.63 | Fretal | -20.40 | 2 | B | S | R | BBC, SW | 9.20 | -0.040 | ZKH |
| 4303 | M61 | 16.1 | | -20.96 | 4 | V | Wat | W | KY | 9.54 | -0.074 | SKSZ |
| 4321 | M100 | 16.1 | Fetal | -21.08 | 4 | V | Wat | W, KB | KY,KBCN | 9.39 | -0.022 | SKSZ |
| 5236 | M83 | 4.5 | Setal | -20.30 | 5 | B | TJD | TA | CELW | 9.24 | -0.025 | ZKH |
| 5457 | M101 | 7.5 | Ketal | -21.19 | 6 | B | S,WKir | KSW | KSW | 9.33 | -0.044 | KG |
| 6946 | | 5.7 | Setal | -20.94 | 6 | B | A | TY | TY | 9.28 | -0.050 | ZKH |
| 7793 | | 3.38 | C | -18.28 | 7 | B | C, VD | CP | (ITB) | 9.05 | -0.134 | ZKH |

List of references to Table 1: A – Ables, 1971; AL – Adler, Liszt, 1989; BBC – Brouillet, Baudry, Combes, 1988; C – Carignan, 1985; CELW – Combes, Encrenaz, Lucas, Weliachew, 1978; CP – Carignan, Puche, 1990; Fetal – Ferrarese et al 1996a,b; FM – Freedman, Madore, 1988; Fretal – Freedman et al., 1994; FWM – Freedman, Wilson, Madore, 1991; Getal – Garnett, Shields, Skillman, Sagan, Dugour, 1997; Hetal – Harnett et al, 1991; HM – Hoessel, Melnick, 1980; ITB – Israel, Tacconi, Baas, 1995; KB – Knapen, Beckman, 1996; KBCN – Knapen, Beckman, Cepa, Nakai, 1996; KDIT – Koper, Dame, Israel, Thaddeus, 1991; Ketal – Kelson et al, 1996; KG – Kennicutt, Garnett 1996; KSW – Kenney, Scoville, Wilson, 1991; KY – Kenney, Young, 1988; LFM – Lee, Freedman, Madore, 1993; N – Newton, 1980; OTK – Okamura, Takase, Kodaira, 1977; R – Rots, 1975; Retal – Ryder, Staveley-Smith, Malin, Walsh, 1995; S – Schweizer, 1976; Setal – Schmidt, Kirshner, Eastman, et al, 1994: SK – Shostak, van der Kruit, 1984; SKSZ – Skillman, Kennicutt, Shields, Zaritsky, 1996; SKT – Sharina, Karachentsev, Tikhonov, 1996; SW – Sage, Westpfahl, 1991; TA – Tilanus, Allen, 1993; TJD – Talbot, Jensen, Dufour, 1979; TW – Thornley, Wilson, 1995; TY – Tacconi, Young, 1986; V – de Vaucouleurs, 1958; V59 – de Vaucouleurs, 1959; V63 – de Vaucouleurs, 1963; VD – de Vaucouleurs, Davoust, 1980; W – Warmels, 1988; Wat – Watanabe, 1983; WK – Walterbos, Kennicutt, 1988; WKA – Wevers, van der Kruit, Allen, 1986; WKir – Whitmore, Kirshner, 1982; WR – Walsh, Roy, 1997; WS – Wilson, Scoville, 1989; ZKH – Zaritsky, Kennicutt, Huchra, 1994.

Note to Table 1:
References in parenthesis are the not detected or negligible small value of molecular hydrogen in the galaxy.

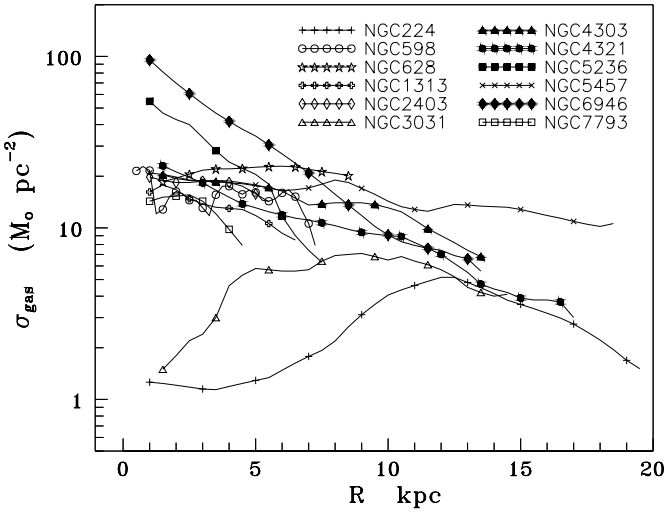


**Fig. 1.** Radial distributions of gas surface mass densities.

The radial distribution of surface gas mass density for the galaxies we consider are shown in Fig. 1.

Because direct measurements of the forbidden-line electron temperature are not available for the HII regions in spiral galaxies, the "empirical" excitation parameter $R_{23} = ([OII] + [OIII])/H\beta$ are used for determination of oxygen abundance. Several workers have suggested calibrations of $R_{23}$ in terms of oxygen abundance (Edmunds & Pagel 1984; McCall & Rybski and Shields 1985; Dopita & Evans 1986; ZKH). ZKH calibration is an average of the three former calibrations. As indicated by Skillman et al (1996), the precise choice of the $R_{23}$ calibration is not critical in differential comparisons of the abundance properties of different objects: this is our main interest in the present study. Oxygen abundance distributions reported in columns 11 and 12 of the Table 1 were obtained with ZKH calibration (for NGC5457 we have recomputed the oxygen abundance using the original $R_{23}$ values from Kennicutt & Garnett 1986 and ZKH calibration) if direct measurements of electron temperature are not available.

### *2.3. The radial distribution of star surface mass density*

The radial distribution of the star surface mass density has been derived from the luminosity profile of the galaxies. The mass to luminosity ratio depends on the star formation history in the galaxy and on the metallicity. To determine the mass to luminosity ratio as a function of the star formation history and of present-day metallicity in gas fraction of a galaxy, a grid of the models of chemical and photometric evolution of one-zone sys-

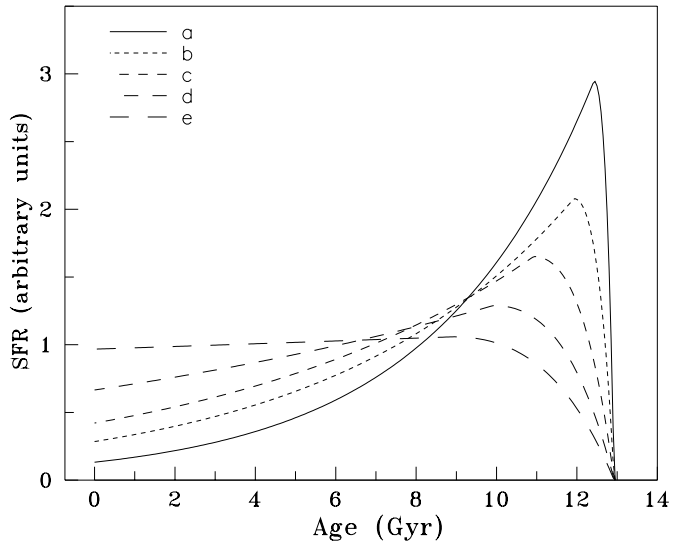


**Fig. 2.** The star formation rate (in arbitrary units) as function of time for the model parameters of Table 2.

**Table 2.** Characteristics of star formation histories.

| SFH | $\tau_{sfr}$ Gyr | $\tau_{top}$ Gyr | SFH | $\tau_{sfr}$ Gyr | $\tau_{top}$ Gyr |
|---|---|---|---|---|---|
| a | 4 | 0.5 | d | 15 | 3 |
| b | 6 | 1 | e | 99 | 4 |
| c | 8 | 2 | | | |

tem has been computed. The key point of the evolution of the system is clearly the star formation rate, $\psi(t)$. We choose to follow the simplest way: the chemical and photometric evolution of one-zone system has been computed for a functional form for $\psi(t)$, which fits the motivated results (see Ferrini and Galli, 1988; Molla et al., 1997) from the previous series of studies by Ferrini and coworkers, where a big effort has been done to justify the physical aspects leading to certain histories of star formation in spiral galaxies. The star formation rate is then described by two time parameters $\tau_{top}$ and $\tau_{sfr}$:

$$\psi(t) \propto \begin{cases} t\ \exp\left(-t/\tau_{top}\right) & \text{if} \quad t \leq \tau_{top} \\ \exp\left(-t/\tau_{sfr}\right) & \text{if} \quad t > \tau_{top}, \end{cases} \qquad (6)$$

The parameters of selected star formation histories are given in Table 2. The star formation rates as function of time, for the different choices of $\tau_{top}$ and $\tau_{sfr}$ based on the results of Molla et al (1997), are shown in Fig. 2. For each star formation history, a grid of models for different present–day gas mass fraction has been computed. Thus, every computed model is specified by the star formation history and the present–day gas mass fraction. The computed parameters of every model relevant to present study are: the present–day oxygen abundance in the gas fraction and the mass to luminosity ratios for the B – band, $M/L_B$, and for the V – band, $M/L_V$.

Based on results of Sandage (1986) and Molla et al (1997), the following correspondence between the Hubble type of the galaxy and its star formation history has been adopted: the a-SFH from Table 2 corresponds to Sab and Sb galaxies (T=2, 3), the b-SFH corresponds to Sbc galaxies (T=4), the c-SFH corresponds to Sc galaxies (T=5), the d-SFH corresponds to Scd galaxies (T=6), and e-SFH corresponds to Sd galaxies (T=7).

**Table 3.** Characteristics of selected variants of oxygen yield.

| Variant | $M_{low}$ $M_\odot$ | $M_{up}$ $M_\odot$ | $\zeta$ | $P_O$ |
|---|---|---|---|---|
| S | 0.05 | 53.5 | 0.289 | 0.0087 |
| W | 0.15 | 110 | 0.461 | 0.0118 |

**Table 4.** Characteristics of the galaxies derived with variant S of oxygen yield.

| NGC No | adopted SFH | M/L $M_\odot/L_\odot$ | $\mu$ | $\eta$ | $\beta_{gas}$ |
|---|---|---|---|---|---|
| 224 | a | 2.39 | 0.042 | 0.538 | 8.06 |
| 598 | d | 1.09 | 0.281 | 0.467 | 2.58 |
| 628 | c | 1.55 | 0.337 | -0.049 | 0.90 |
| 1313 | e | 0.91 | 0.366 | 0.464 | 2.71 |
| 2403 | d | 0.97 | 0.394 | 0.567 | 3.01 |
| 3031 | a | 2.35 | 0.067 | 0.563 | 6.21 |
| 4303 | b | 1.91 | 0.140 | 0.180 | 1.62 |
| 4321 | b | 1.98 | 0.102 | 0.001 | 1.01 |
| 5236 | c | 1.71 | 0.119 | 0.092 | 1.28 |
| 5457 | d | 1.21 | 0.313 | 0.043 | 1.10 |
| 6946 | d | 1.25 | 0.176 | 0.193 | 1.62 |
| 7793 | e | 0.88 | 0.280 | 0.415 | 2.29 |

The chemical and photometric evolution of one-zone system has been computed with temporal step as large as 50 Myr. At every temporal step a star generation is produced, and the mass of star generation is defined by the adopted star formation history. The contribution of each generation of stars to the chemical enrichment of the interstellar medium is governed by the prescription for the production of new elements by individual stars as well as by the stellar initial mass spectrum. The oxygen yield has been computed with the production of oxygen by individual stars from Maeder (1992) (cases with and without stellar winds have been considered) and with Salpeter initial mass spectrum (Salpeter 1955). Two variants of oxygen yield have been considered. The production of oxygen by individual stars as predicted by the stellar models without stellar winds (Maeder 1992) has been adopted in the first variant which will be referred to as S variant. The adopted parameters ($M_{low}$ – lower and $M_{up}$ – upper mass limits of the initial mass function) and computed characteristics ($P_O$ – oxygen yield, $\zeta$ – fraction of mass of single stellar population which is contained in stars with masses above $1M_\odot$) are listed in Table 3. The production of oxygen by individual stars as predicted by the stellar models with stellar winds (Maeder 1992) has been adopted in the second variant which will be referred to as W variant. The adopted and computed characteristics for this variant are also listed in Table 3. The data of Renzini & Voli (1981) for intermediate and low mass stars has been used in both variants.

The photometric evolution of a system has been computed using the data for the single stellar populations of different

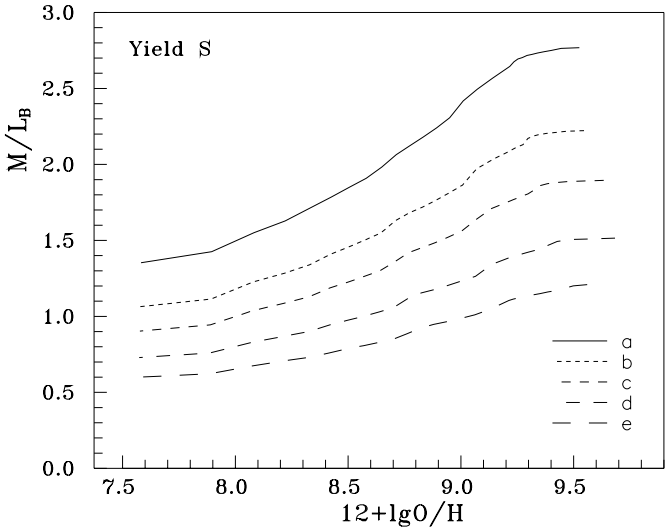


**Fig. 3.** $M/L_B$ ratios computed with variant S of oxygen yield as a function of the present-day oxygen abundances in gas phase for different choices of star formation history from Table 2.

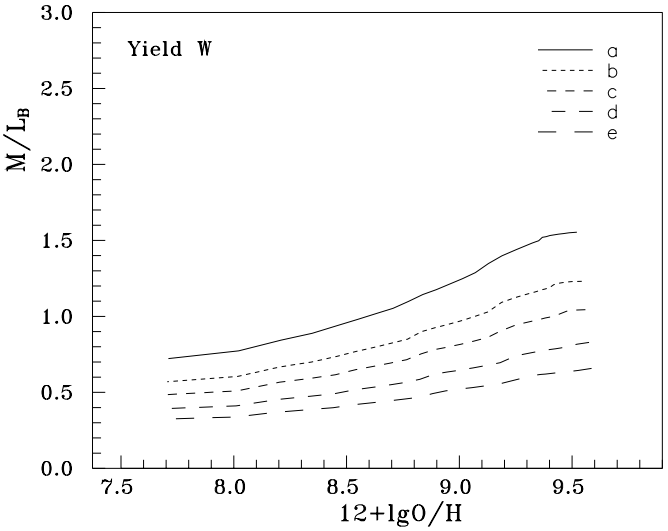


**Fig. 4.** $M/L_B$ ratios computed with variant W of oxygen yield as a function of the present-day oxygen abundances in gas fraction for different choices of star formation history from Table 2.

**Table 5.** Characteristics of the galaxies derived with variant W of oxygen yield

| NGC No | adopted SFH | M/L $M_\odot/L_\odot$ | $\mu$ | $\eta$ | $\beta_{gas}$ |
|---|---|---|---|---|---|
| 224 | a | 1.24 | 0.079 | 0.547 | 6.80 |
| 598 | d | 0.57 | 0.430 | 0.401 | 1.94 |
| 628 | c | 0.80 | 0.496 | -0.209 | 0.72 |
| 1313 | e | 0.48 | 0.522 | 0.378 | 2.02 |
| 2403 | d | 0.51 | 0.555 | 0.492 | 2.21 |
| 3031 | a | 1.22 | 0.120 | 0.556 | 5.06 |
| 4303 | b | 1.00 | 0.237 | 0.142 | 1.36 |
| 4321 | b | 1.04 | 0.179 | -0.004 | 0.99 |
| 5236 | c | 0.88 | 0.208 | 0.070 | 1.17 |
| 5457 | d | 0.63 | 0.467 | -0.094 | 0.88 |
| 6946 | d | 0.65 | 0.292 | 0.139 | 1.34 |
| 7793 | e | 0.46 | 0.428 | 0.340 | 1.75 |

metallicities from Tantalo et al (1996). The data for luminosity from Tantalo et al (1996) has been rescaled according to the value of $\zeta$ depending on the adopted variant of oxygen yield, see Table 3. The $M/L_B$ ratios computed for the case S of oxygen yield are represented in Fig. 3 as a function of the present-day oxygen abundances in gas phase for different choices of star formation history. The results for the case W of oxygen yield are shown in Fig. 4.

The radial distributions of surface brightness are reported in the literature in different forms: the observed luminosity profile along the major axis (de Vaucouleurs 1958, 1959; Hoessel & Melnick 1980; Walterbos & Kennicutt 1988), the azimuthally averaged luminosity profile (Schweizer 1976, Okamura et al 1977, Talbot et al 1979, Carignan 1985), and generalized radial luminosity profile (Watanabe 1983). Using traditionally accepted approach (disk-spheroid decomposition), the radial luminosity profile of each type has been approximated by the expression

$$I(r) = I_e \exp\left(-3.33[(r/r_e)^{1/4} - 1]\right) + I_0 \exp\left(-r/r_0\right), \quad (7)$$

where $I_e$ and $I_0$ are brightness-scale parameters, $r_e$ and $r_0$ are the length-scale parameters of the spheroid and the disk, respectively.

The observed surface brightness has been corrected for Galactic extinction. The values of $A_B$ have been taken from RC3. When the luminosity profile in V band is used, the value of $A_V$ has been found as $A_V = A_B/1.337$ (Cardelli et al 1989). Then the surface brightness has been corrected for internal extinction $A_i$, taken from RC3. As a rough approximation, $A_i$ has been adopted constant over the body of the galaxies. Fortunately, the values of $A_i$ for considered galaxies are rather small: only in three cases (NGC224, 598, 3031) the values of $A_i$ are in excess of 0.25, i.e. only for three galaxies correction for internal extinction results in the variation of luminosity more than 25 percent. Then the radial luminosity profile has been corrected, if necessary, to a face-on value, using a purely geometrical correction for inclination, $-2.5\log(\cos i)$. The radial distributions of star surface mass densities, derived using a face-on luminosity profiles and mass to luminosity ratios for case S of oxygen yield, are presented in Fig. 5. The value of radius, at which corrected for Galactic and internal extinction face-on surface brightness in B band is equal to 25 $mag\,arcsec^{-2}$, has been adopted as a boundary for the galaxy. In the case of V band, the boundary of galaxy has been defined as a radius, at which the brightness is equal to 24.5 $mag\,arcsec^{-2}$, taking into account that B-V $\sim 0.5$ for these galaxies. The radial distributions of star surface mass densities, derived using a face-on luminosity profiles and mass to luminosity ratios for case W of oxygen yield, are presented in Fig. 6.

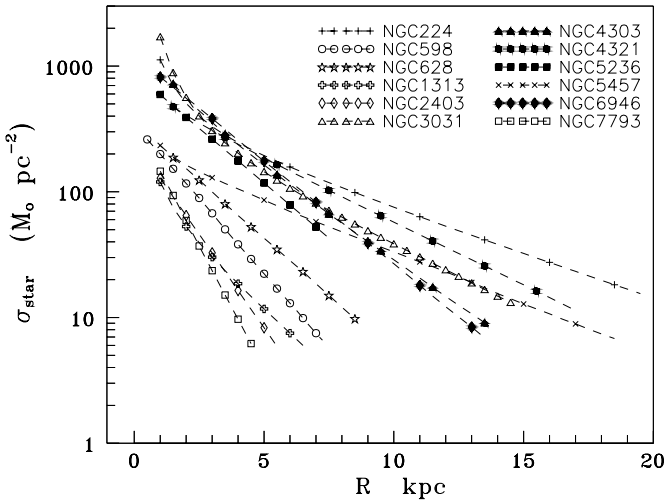


**Fig. 5.** The radial distributions of star surface mass densities for galaxies derived for the case S of oxygen yield.

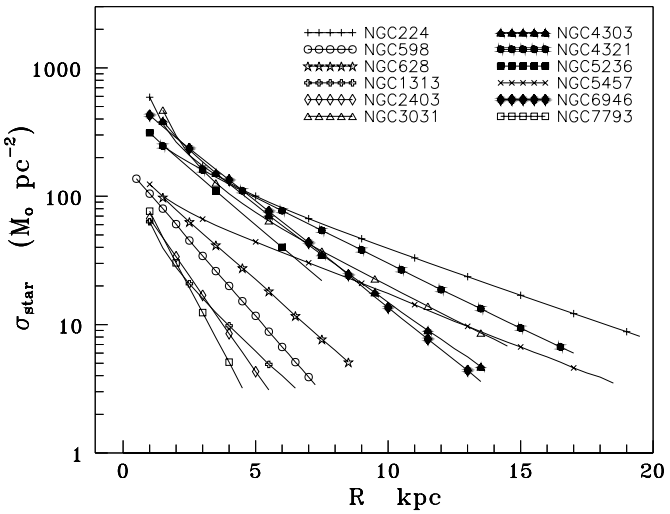


**Fig. 6.** The radial distributions of star surface mass densities for galaxies derived for the case W of oxygen yield.

The position of every galaxy in the $\mu$ versus O/H diagram computed for case S of oxygen yield is shown in Fig. 7. The results for case W of oxygen yield are presented in Fig. 8.

## 3. Results and discussion

### *3.1. Oxygen yield and oxygen abundance deficiency*

Characteristics of galaxies computed for the case S of oxygen yield are given in Table 4. The NGC number is listed in column 1. The adopted star formation history (from Table 2) is reported in column 2. The global mass to luminosity ratio (ratio of total mass of stars within considered boundary of galaxy to total luminosity within this radius) is given in column 3. The global gas mass fraction within considered boundary is reported in column 4. The value of oxygen abundance deficiency is listed in column 5. The parameter $\beta_{gas}$ is reported in column 6. The parameter $\beta_{gas}(r)$ is defined as $\beta_{gas}(r) = \sigma^{CB}_{gas}(r)/\sigma_{gas}(r)$,

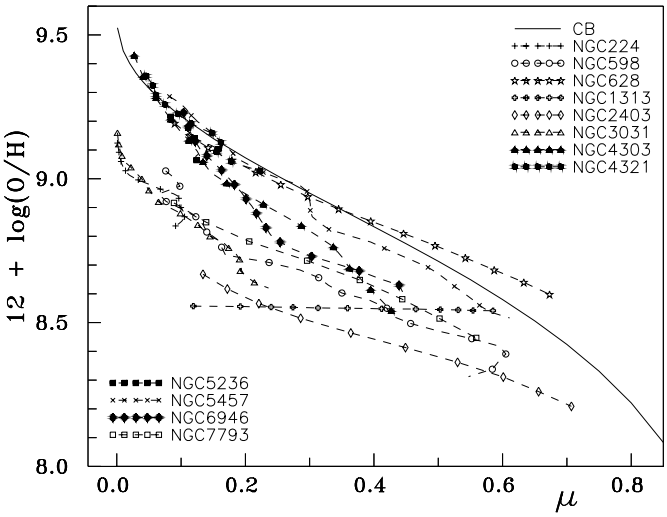


**Fig. 7.** The positions of galaxies and closed-box models with different values of the present-day gas mass fraction in the $\mu - O/H$ diagram for the case S of oxygen yield.

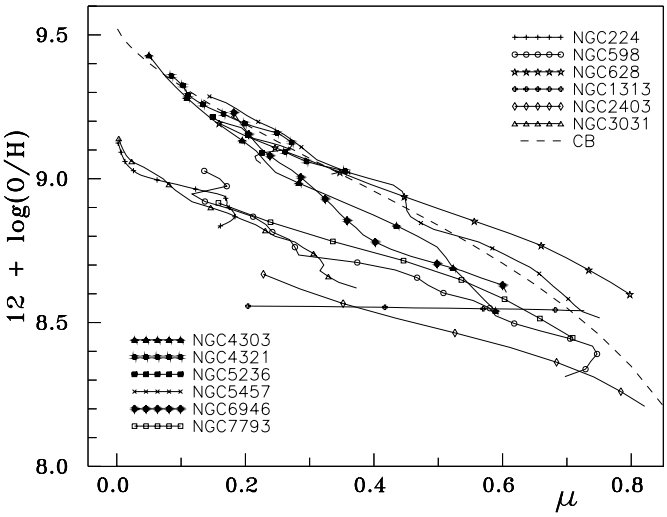


**Fig. 8.** The positions of galaxies and closed-box models with different values of the present-day gas mass fraction in the $\mu - O/H$ diagram for the case W of oxygen yield.

where $\sigma_{gas}(r)$ is the gas surface mass density at a given radius in the galaxy, and $\sigma^{CB}_{gas}(r)$ is the gas surface mass density of the closed-box model for a given oxygen abundance and a given star surface mass density. The parameter $\beta_{gas}(r)$ indicates how much the gas surface mass density at a given radius in the galaxy must be increased (decreased) in order that the O/H(r) – $\mu$(r) relation would be in agreement with closed-box mode l predictions. In the present study, the only application of the parameter $\beta_{gas}(r)$ is as follows: the parameter $\beta_{gas}(r)$ tells something about the reality of gas mass fraction deficit (excess) at a given radius in the galaxy. The va lue of global gas mass deficit (excess) in the galaxy $\beta_{gas} = M^{CB}_{gas}/M_{gas}$ is reported in Table 4 (column 6).

Characteristics of galaxies computed for the case W of oxygen yield are given in Table 5.

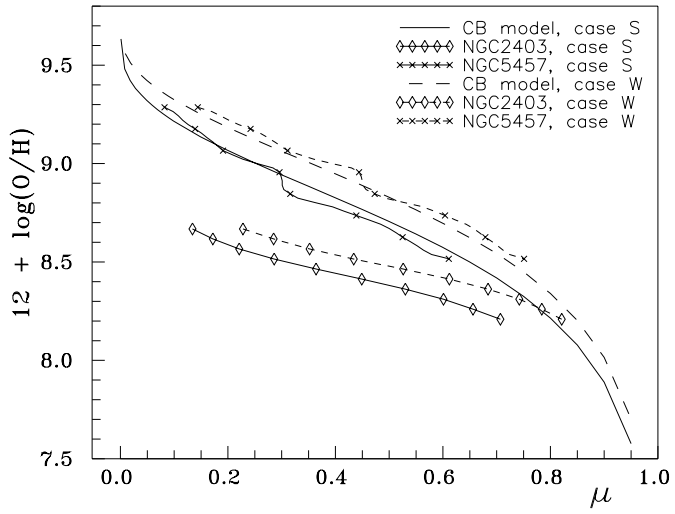


**Fig. 9.** The positions of closed-box models with different values of the present-day gas mass fraction (solid line), NGC2403 (solid line with rhombuses), NGC5457 (solid line with crosses) in the $\mu - O/H$ diagram for the case S of oxygen yield. The positions of closed-box models (dashed line), NGC2403 (dashed line with rhombuses), NGC5457 (dashed line with crosses) for the case W of oxygen yield.

The derived value of the gas surface mass density in the galaxy is a model-independent value. On the contrary, the derived value of the star surface mass density is strongly dependent on the adopted variant of oxygen yield due to the significant difference in mass to luminosity ratios for cases S and W of oxygen yield (compare Figs. 3 and 4, or data of Tables 4 and 5). As a result, the derived value of the gas mass fraction in a galaxy is also a model-dependent value, Table 4 and 5. Therefore, not only the position of the closed-box model in the $\mu$ – O/H diagram but also the positions of galaxies in this diagram are dependent on the choice of the variant of oxygen yield. It can be easily seen in Fig. 9. The positions of the closed-box models with different values of the present-day gas mass fraction computed with variant S of oxygen yield are shown in Fig. 9 by solid line. The positions of galaxies NGC2403 and NGC5457 computed with variant S of oxygen yield are shown in Fig. 9 by solid lines labeled by rhombuses and crosses, correspondingly. The positions of the closed-box models and galaxies NGC2403 and NGC5457 computed with variant W of oxygen yield are shown in Fig. 9 by dashed line without labels and dashed lines labeled by rhombuses and crosses, correspondingly.

Whereas the positions of a galaxy in the $\mu$ – O/H diagram are appreciably different in the cases of S and W of oxygen yield, the displacements of galaxy positions relative to corresponding closed-box models (or displacement of position of one galaxy relative to the other galaxy) are similar for both cases of oxygen yield, Fig. 9 (compare also Figs. 7 and 8), i.e. the values of oxygen abundance deficiency derived in cases S and W of oxygen yield are relatively close to each other, Tables 4 and 5. As it was indicated above, the closed-box model gives the upper limit of oxygen abundance in the system with fixed value of gas mass fraction. In other words, the area above the positions of one-zone closed-box models with different values of the present-day gas mass fraction in the $\mu$ – O/H diagram is a forbidden area for galaxies. Then the lower and upper mass limits of the initial mass function in cases S and W of oxygen yield have been chosen in such manner that the minimum values of $\eta$ for galaxies were around zero, i.e. that galaxies are not located in the forbidden area. For a fixed upper (lower) mass limit of the initial mass function the decrease of the lower (upper) mass limit results in that some galaxies will be located in the forbidden area, they will have negative (significantly different from zero) values of $\eta$. For a fixed upper (lower) mass limit of the initial mass function the increase of the lower (upper) mass limit results in that all the galaxies will have large positive values of $\eta$. However, for any choice of the parameters of the initial mass function the difference between the values of the oxygen abundance deficiency for two galaxies will not be significantly changed. Thus, the precise choice of the oxygen production by individual stars and of parameters of the initial mass function is not very critical in differential comparisons of the oxygen abundance deficiency of different galaxies. Therefore, only the results obtained with case S of oxygen yield will be discussed below.

### *3.2. On the reality of oxygen abundance deficiency*

As it can be seen from Fig. 7, four galaxies (NGC 628, 4321, 5236, and 5457) are located in the $\mu$ – O/H diagram close to the curve defined by the one-zone closed-box models with different gas mass fraction (this curve will be referred to as standard curve). The values of $\eta$ of these galaxies are close to zero, i.e. the values of oxygen abundance deficiency (or excess) are less than 0.1, Table 4. These galaxies will be referred to as galaxies without oxygen abundance deficiency, although small values of oxygen abundance deficiency for these galaxies cannot be excluded taking into account the low precision of ava ilable observational data.

The inner parts of two galaxies (4303 and 6946) are also located close to the standard curve, while outer parts of these galaxies show an appreciable displacement relative to the standard curve. While the very inner part of NGC4303 shows a small excess of oxygen abundance, the outer part (from $\sim$ 5 kpc to 13.5 kpc – adopted boundary of the galaxy) shows an oxygen abundance deficiency. The value of local oxygen abundance deficiency increases with increasing of galactocentric distance and reaches a value around 0.45 at the boundary. The behavior of the value of local oxygen abundance deficiency in NGC6946 is similar. The values of global oxygen abundance deficiency in NGC4303 and in NGC6946 are rather moderate: $\eta$=0.18 for NGC4303 and $\eta$=0.19 for NGC6946, Table 4. These galaxies will be referred to as galaxies with moderate oxygen abundance deficiency.

The values of global oxygen abundance deficiency for galaxies with moderate oxygen abundance deficiency differ slightly from gala xies without oxygen abundance deficiency. The minor difference in global oxygen abundance deficiency cannot justify their division into two classes. The base of the division

into these two classes is readily apparent from the behaviour of the value of lo cal oxygen abundance deficiency. In galaxies named galaxies without oxygen abundance deficiency, the value of local oxygen abundance deficiency is small for any region of the galaxy, Fig. 7. In galaxies named galaxies with moderate oxygen abundance defi iency, there is an appreciable oxygen abundance deficiency in the outer part of a galaxy while the inner part has no oxygen abundance deficiency (see discussion above as well as Fig. 7). This justifies the division into the two classes.

Positions of ne-half of galaxies from our list (NGC224, 598, 1313, 2403, 3031, and 7793) in the $\mu$ – O/H diagram show significant displacements as compared to the position of the standard curve, Fig. 7. The values of $\eta$ for these galaxies are in the range from $\sim$ 0.4 to $\sim$ 0.55. Can the displacements of positions of these galaxies be caused by uncertainties in the determinations of the values of oxygen abundance or/and of gas mass fraction? Let us compare the galaxies NGC2403 and NGC5457. These galaxies, with the same Hubble type (Scd, T=6), have very different values of $\eta$, Table 4. Comparison of these galaxies can tell something about the reality of the oxygen abundance deficiency in galaxies.

The difference in oxygen abundances between these galaxies increases from $\Delta$[O/H] $\sim$ 0.2 for $\mu$=0.6 to $\Delta$[O/H] $\sim$ 0.5 for $\mu$=0.15, Fig. 9. The oxygen abundances in HII regions of NGC2403 have been determined using direct measurements of electron temperature. The errors of oxygen abundance determinations for individual HII regions are not in excess of 0.1 dex, and the error in the oxygen abundance gradient is 0.009 dex/kpc (Garnett et al 1997). The oxygen abundances in HII regions of NGC5457 have been determined using calibration of the $R_{23}$ excitation parameter. As it was indicated above, the oxygen abundance data obtained with ZKH calibration, which is an average of calibrations of Edmunds & Pagel (1984), McCall, Rybski and Shields (1985), and Dopita & Evans (1986), has been used in present study. All the calibrations give, in fact, the same oxygen abundances for low metallicity HII regions in the outer part of the NGC5457, while the differences between oxygen abundances of high metallicity HII regions in the inner part obtained with ZKH and other calibrations can be about 0.2 dex. The observational errors contribute negligibly to the error due to the choice of the calibration (Kennicutt & Garnett 1996). Thus, the difference in the oxygen abundances in HII regions in NGC2403 and in NGC5457 for a given value of gas mass fraction is in excess of inexactness due to observational errors or due to the uncertainties in the $R_{23}$ calibration. This difference is likely to reflect real difference in oxygen abundance for NGC2403 and NGC5457, although the exact value of the difference in the oxygen abundance depends on the choice of the $R_{23}$ calibration.

If the displacement in position of NGC2403 relatively to NGC5457 (or to the standard curve) is caused by an error in the gas mass fraction determination, then the gas surface mass density in NGC2403 is underestimated by a factor of $\sim$ 1.5 at 5.5 kpc and by a factor of $\sim$ 7 at 1 kpc (with value of $\beta_{gas} \sim 3$ for the whole galaxy, Table 4). Or the star surface mass density is overestimated to the same extent since $\beta_{star} = 1/\beta_{gas}$. In order to bring the position of NGC2403 in the $\mu$ – O/H diagram in coincidence with the position of NGC5457 (or standard curve), the mass to luminosity ratio in NGC2403 at 1 kpc should be decreased by a factor of 7 (up to $M/L_B \sim 0.15$) or $H_2$ to CO conversion factor should be increased by a factor of about 15 (up to $X^* \sim 60$), leaving the corresponding values for NGC5457 unaltered. So large variations of $M/L_B$ and $X^*$ among galaxies of the same Hubble type seem to be unrealistic.

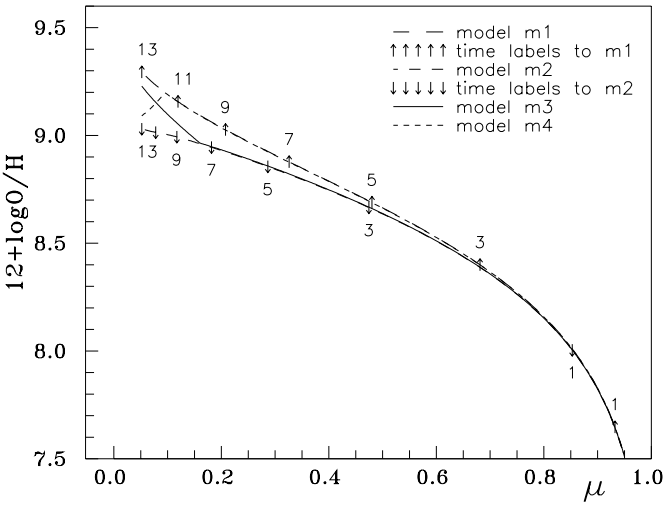


**Fig. 10.** The evolutionary tracks of models m1, m2, m3, and m4 in the $\mu$ – O/H diagram (see text). The positions of the models m1 and m2 at fixed times are indicated.

Thus, the differences in positions of galaxies in the $\mu$ – O/H diagram seem to be not caused by uncertainties in the determination of oxygen abundance or/and of gas fraction but seem to reflect a real difference in the properties of galaxies.

### *3.3. Galaxies without oxygen abundance deficiency*

It is well known that the closed-box model of galactic chemical evolution predicts many more low-metallicity stars than are observed in the solar neighbourhood. Various versions of the infall model, in which an infall of gas onto the disk takes place for a long time, have been suggested (Tosi 1988a,b; Matteucci & François 1989; Ferrini et al 1992; Pardi & Ferrini 1994; Pagel & Tautvaisiene 1995; Pilyugin & Edmunds 1996). An infall model has also been applied to other spiral galaxies (Diaz & Tosi 1986; Molla et al 1996, 1997). Thus, it is generally agreed that a gas infall can play an important role in the chemical evolution of disks of spiral galaxies. Moreover, the effects of accretion are visible in NGC5457 (as high velocity gas features) (Kamphuis & Sancisi 1994). Therefore, the fact that the positions of a number of galaxies (including NGC5457) are close to the position of standard curve may appear surprising.

In order to illustrate the gas infall effects on the chemical evolution of a system, we will consider the simplest infall model which is specified by the ratio of gas infall rate to star formation rate, $\kappa$; the value of $\kappa$=0 corresponds to the closed-box model.

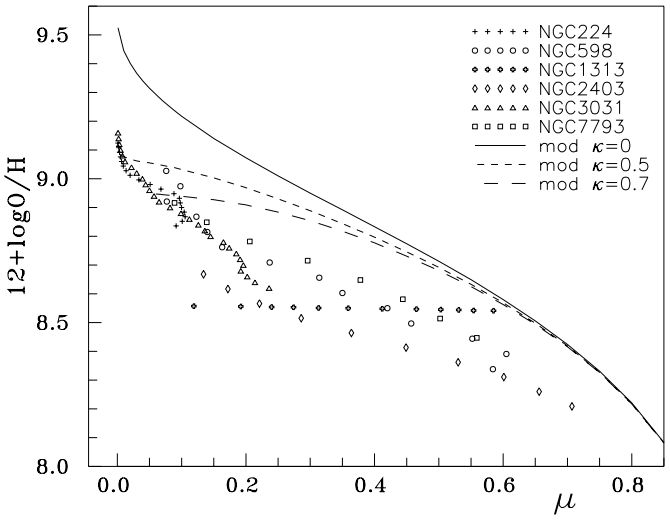


**Fig. 11.** The positions of galaxies with oxygen abundance deficiency and models with $\kappa$ =0, 0.5, and 0.7 in the $\mu$ – O/H diagram.

The value of $\kappa$ =0.7 corresponds approximately to the case when the gas infall compensates the gas exhaustion due to conversion into stars (note that a fraction around 0.2 of mass of each star generation returns back to the interstellar medium for case S of oxygen yield). The evolutionary tracks of the closed-box model m1 and the infall model m2 with $\kappa$=0.5 in the $\mu$ - O/H diagram are presented in Fig. 10. It can be seen that an appreciable difference between these tracks takes place in the range of low values of $\mu$ only. The infall of unenriched gas influences the chemical evolution of a system (in particular, the abundance distribution function) not via the change of the evolutionary tracks in the $\mu$ - O/H diagram but mainly through the change of the rate of evolution along the tracks. This can be easily seen in Fig. 10 where the positions of the system at fixed moments of time are shown both for the closed-box and for the infall models. The gas infall results in displacement of the position of a galaxy from the closed-box model position in the $\mu$ – O/H diagram when the amount of infalling gas is comparable to the amount of gas in the system. Therefore, it is not surprising that NGC5457 is located close to the standard curve since the total HI mass in high velocity gas complexes is only one percent of the HI mass in the galaxy (Kamphuis & Sancisi 1994).

The evolutionary track of model m3, which evolves with $\kappa$=0.5 for the first 10 Gyr and then evolves with $\kappa$=0 for the last 3 Gyr, is shown in Fig. 10. The present-day position of model m3 is close to the position of the closed-box model m1. It should be noted that although model m3 evolves along the track of model m2 for 10 Gyr, the positions of models m3 and m2 on the track at fixed time (say, 10 Gyr) do not coincide. The evolutionary track of model m4, which evolves with $\kappa$=0 for the first 10 Gyr and then evolves with $\kappa$=0.5 for the last 3 Gyr, is also presented in Fig. 10. The present-day position of model m4 is close to the position of model m2. Thus, the present-day position of a system in the $\mu$ – O/H diagram is governed by its evolution in the recent past and is, in fact, independent on its evolution in the distant past. Therefore, the fact that the present-day positions of a number of galaxies are close to the positions of the closed-box models is not in conflict with that the model, in which an infall of gas onto the disk takes place for a long time, is necessary to satisfy the observed abundance distribution function and age-metallicity relation in the solar neighbourhood since these observational data reflect the evolution of a system in the distant past.

### *3.4. Galaxies with large values of $\eta$*

The galaxies which have large values of $\eta$ can be divided into two groups. The first group contains two large spirals of early types: NGC224 (T=3) and NGC3031 (T=2). The second group contains four low luminosity spirals of late types: NGC598 (T=6), NGC1313 (T=7), NGC2403 (T=6), and NGC7793 (T=7). At the outset the first group of galaxies will be considered.

The positions of NGC224 and NGC3031 together with positions of models with $\kappa$=0, 0.5, 0.7 are presented in Fig. 11. Fig. 11 shows that the position of NGC224 (except the external parts with galactocentric distances in excess of $\sim$ 15 kpc) corresponds to positions of models with low or moderate rate of gas infall. The prominent feature of NGC224 is a low value of gas mass fraction, Table 4, due to low surface gas mass density, Fig. 1. In the inner part (within $\sim$ 6.5 kpc) the value of $\mu$ is below 0.01. For such low values of $\mu$ the manifestation of the well known effect of reducing the oxygen abundance in the gas component of the galaxy due to mass ejection by old low-metallicity stars can be expected. Figs. 12 and 13 demonstrate the manifestation of this effect. Models n1 and n2 have the same present-day gas mass fraction $\mu$=0.006. In model n1, the amount of gas in the system is a monotonically decreasing function of time due to continuous star formation. In the case of low gas surface mass density (1-2 $\mathrm{M_\odot\,pc^{-2}}$ in the inner part of NGC224) the model with continuous star formation seems not a justified approximation. Then, in the model n2 we consider a system in which the gas is exhausted for 11.5 Gyr; at that time the star formation stops, and the amount of gas in the system increases due to mass ejection by stars, Fig. 12. Models n1 and n2 have the same present-day gas mass fraction, but the oxygen abundance in gas fraction of model n2 is almost twice below than in model n1, Fig. 13. Models n3 and n4 are similar to models n1 and n2 in some sense, but they have the present-day gas mass fraction $\mu$=0.05, Fig. 12. In this case the decrease of oxygen abundance in gas fraction of system due to mass ejection by old stars is negligibly small, Fig. 13.

Thus, in the case of system with extremely low value of gas mass fraction, the oxygen abundance predicted by the closed-box model is strongly dependent on the adopted star formation history. Therefore, it should be taken into account that the determinat ion of oxygen abundance deficiency in region of a galaxy with extremely low value of gas mass fraction can contain a large error, i.e. a part (may be major) of derived oxygen abundance deficiency can be artificial because of difference between adopted and real star formation history in a galaxy.

Since a continuous star formation has been adopted in the computation of standard curve, the real value of oxygen abun-

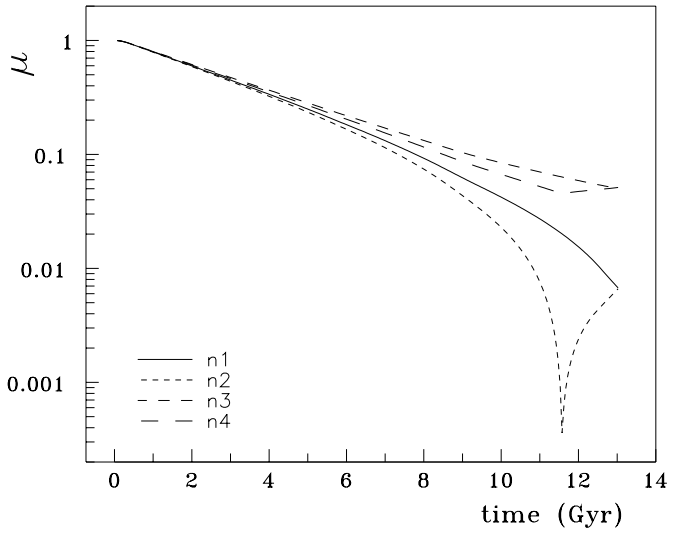


**Fig. 12.** The gas mass fraction in models n1, n2, n3, and n4 as a function of time (see text).

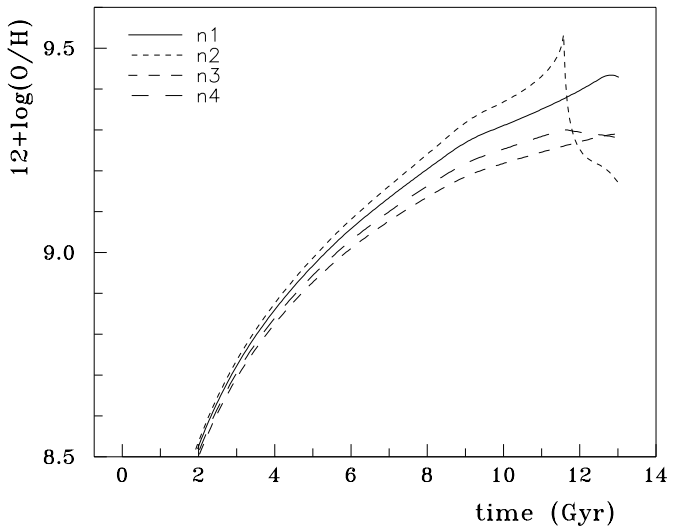


**Fig. 13.** The oxygen abundance in models n1, n2, n3, and n4 as a function of time (see text).

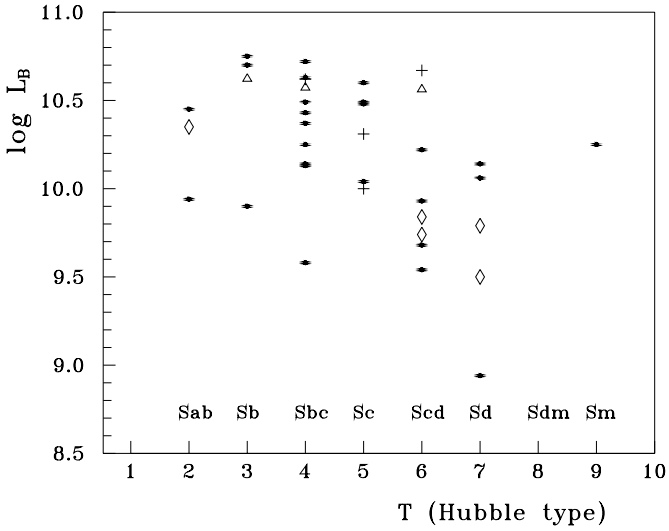


**Fig. 14.** The positions of galaxies in the blue luminosity versus Hubble type diagram. The galaxies from the present study are shown with rhombuses (galaxies with large oxygen abundance deficiency), with triangles (galaxies with moderate oxygen abundance deficiency), with pluses (galaxies without oxygen abundance deficiency). The galaxies from ZKH (without determinations of values of oxygen abundance deficiency) are represented by points. The same symbols will be used in Figs. 15 and 16.

dance deficiency in the inner part of NGC224 can be lower (if any) than was obtained from comparison with the standard curve, and it is quite possible that the gas exchange with environments in the recent past should be assumed in order to reproduce the observed oxygen abundance in the outer part of NGC224 only. In other words, the real value of oxygen abundance deficiency in NGC224 seems to be comparable with that in NGC4303 and NGC6946. Then the NGC224 is assumed to be a galaxy with moderate oxygen abundance deficiency, although this conclusion is not beyond question. A model of chemical evolution with accurately determined star formati on history should be constructed for the NGC224 in order to clarify whether the low oxygen abundance in the inner part of this galaxy is conditioned by large contribution of mass ejection by old low-metallicity stars to gas fraction or is caused by gas e xchange between inner parts of the galaxy and its environments (including the outer part of the galaxy).

Fig. 11 shows that a significant part of NGC3031 is located below the positions of models with $\kappa$ =0.5, 0.7. Since NGC3031 has a low surface gas mass density within only $\sim$ 3 kpc, Fig. 1, the contribution of the reduction of the oxygen abundance in gas fraction of galaxy due to mass ejection by old stars to oxygen abundance of NGC3031 cannot be large. Therefore, we have to conclude that there is a significant gas exchange between this galaxy and the environment or/and a significant redistribution of gas (heavy elements) within the disk. In the case of NGC3031 such conclusion is in the line with fact that NGC3031 is clearly interacting with its two neighbouring galaxies NGC3034 (M82) and NGC3077: bridges of gas connect NGC3031 to NGC3034 and NGC3077 (van der Hulst 1979, Brouillet et al 1991, Thomasson & Donner 1993).

The positions of low luminosity late-type spirals (NGC598, 1313, 2403, and 7793) in the $\mu$ – O/H diagram, Fig. 11, are strong evidence that there are significant gas exchange between these galaxies and their environments. The heavy elements loss via galactic winds rather than the infall of unenriched gas onto the galaxy is a reason of oxygen abundance deficiency in these galaxies. First, the oxygen abundances in these galaxies could be reproduced only by the models with $\kappa > 0.7$. In this case, however, the gas mass in the system increases with time and the metallicity of stars exceeds the present-day metallicity of gas, which is in contradiction with observational data. Second, the reduced oxygen abundance in combination with high iron to oxygen abundance ratio observed in the Large Magellanic Cloud (which is comparable to low luminosity spirals in luminosity and

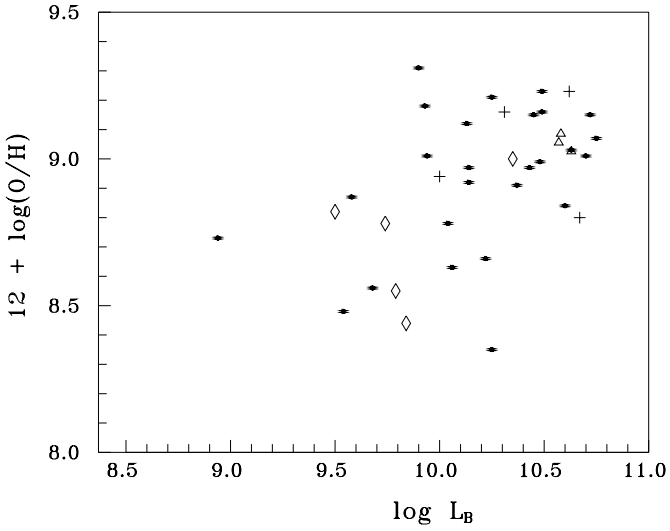


**Fig. 15.** The positions of galaxies in the blue luminosity versus oxygen abundance diagram. The characteristic oxygen abundance is the oxygen abundance at $r^* = 0.4\rho_0$, where $\rho_0$ is the isophotal radius.

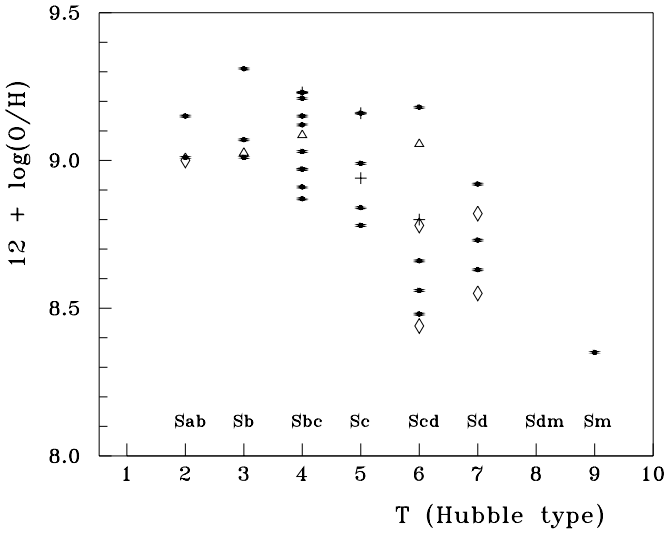


**Fig. 16.** The positions of galaxies in the Hubble type versus oxygen abundance diagram. The characteristic oxygen abundance is the oxygen abundance at $r^* = 0.4\rho_0$, where $\rho_0$ is the isophotal radius.

has a disk-like structure) can be well reproduced by the model with galactic winds (Pilyugin 1996).

### *3.5. Oxygen abundance deficiency and properties of spiral galaxies*

Most properties of galaxies depend on either Hubble type (for example, the star formation history in the galaxy) or luminosity (or mass). Therefore, the possibility that the oxygen abundance deficiency correlates with these quantities will be examined here. Fig. 14 shows the positions of galaxies in the Hubble type versus blue luminosity diagram. The rhombuses, triangles, plus correspond respectively to the galaxies with large, moderate, null oxygen abundance deficiency. The galaxies from ZKH which have no determination of the oxygen abundance deficiency are represented by points. The positions of galaxies in the blue luminosity versus characteristic oxygen abundance diagram and in the Hubble type versus characteristic oxygen abundance diagram are shown in Figs. 15 and 16, respectively. The same symbols as in the Fig. 14 are used. The oxygen abundance at $r^* = 0.4\rho_0$, where $\rho_0$ is the isophotal radius, have been used as the characteristic oxygen abundance in the galaxy. Although the interacting galaxy NGC3031 is presented in every diagram, this galaxy will not be taken into consideration below.

From Figs. 14-15 it can be seen that all low-luminosity late-type spirals in our sample have significant values of oxygen abundance deficiency while high-luminosity spirals have no, or have moderate oxygen abundance deficiency, although among high-luminosity spirals the oxygen abundance deficiency does not correlate with luminosity or Hubble type. It should also be noted that the radial distribution of local oxygen abundance deficiency varies in passing from high to low luminosity spirals. The oxygen abundance deficiency in high luminosity spirals takes place only in the outer part of a galaxy while the inner part has no oxygen abundance deficiency. On the contrary, in low luminosity spirals it takes place over the whole body of galaxy: moreover, the value of local oxygen abundance deficiency has a maximum in the inner part of the galaxy. Since the oxygen abundance deficiency in the region of a galaxy is caused by the mass exchange between given region and its environment, we can conclude that at the present epoch the mass exchange with environments or gas (heavy elements) redistribution within disk play a more important role in the chemical evolution of low-luminosity late-type spirals than in high luminosity spiral galaxies. Our results are in the line with the conclusions of Binggeli (1994) that the transition from late-type giants to late-type dwarfs has occurred at the late end of Hubble sequence and that the mass loss by galactic winds is an underlying physical cause of this transition. Following the definition of late-type giants versus late-type dwarfs dichotomy by Binggeli (1994) "dwarf galaxies did, classical (giant) galaxies did not, suffer global mass loss by galactic winds", the spiral galaxies NGC598, NGC1313, NGC2403, and NGC7793 belong to dwarf galaxies.

Inspection of Figs. 15-16 suggests that the characteristic oxygen abundance is not an indicator of the oxygen abundance deficiency.

At present time the oxygen abundance deficiency can be determined for a small number of galaxies. In order to confirm or change our conclusions a large number of galaxies spanning the whole ranges of luminosity and Hubble type should be considered.

## 4. Conclusions

The observed radial distributions of oxygen abundance in a number of spiral galaxies of different Hubble types from Sab to Sd have been compared with predictions of the closed-box model for chemical and photometric evolution of galaxies, with the purpose of searching for the deficiency of oxygen abundance

in galaxies, which is an indicator of mass exchange between the galaxy and its environments or radial redistribution of gas (heavy elements) within disk.

It has been found that, within our limited sample, among the high luminosity spiral galaxies, only NGC3031 (M81) – a well known interacting galaxy – has a large oxygen abundance deficiency. Other high luminosity galaxies of Hubble types from Sbc to Scd have no, or have a moderate deficiency of oxygen abundance. All the low luminosity Scd and Sd galaxies in our sample show a significant deficiency of oxygen abundance.

It has been obtained that the high luminosity spiral galaxies without oxygen abundance deficiency are located in the $\mu$ – O/H diagram close to the curve which is described by positions of one-zone closed-box models with different values of the present-day gas mass fraction. It has been shown that this is not in conflict with the fact that the infall model is necessary to satisfy observational data for spiral galaxies, in particular, observational data for the solar neighbourhood.

It has been found that high luminosity spiral galaxies with moderate oxygen abundance deficiency and low luminosity spirals with large oxygen abundance deficiency are distinguished not only by the values of global oxygen abundance deficiency but also by the radial distributions of local oxygen abundance deficiency. The oxygen abundance deficiency in high luminosity spirals takes place only in outer part of a galaxy while in low luminosity spirals the oxygen abundance deficiency takes place over the whole body of the galaxy.

Large values of oxygen abundance deficiency obtained for all low luminosity Scd and Sd galaxies can be considered as an evidence in favor of that these galaxies lost the heavy elements in course of their evolution. This result is in the line with the conclusions of Binggeli that the transition from late-type giants to late-type dwarfs occurs at the late end of the Hubble sequence and that the mass loss via galactic winds is an underlying physical cause of this transition.

*Acknowledgements.* We thank the referee, Prof. B.E.J. Pagel, for his constructive comments on the manuscript. L.P. thanks the Staff of Department of Physics, Section of Astronomy (University of Pisa) for hospitality, the CNR for financial support of a visit to Italy.

## References

Ables H.D., 1971, Publications of the United States Naval observatory, second series, v XX, part 4
Adler D.S., Liszt H.S., 1989, ApJ 339, 836
Alves D.R., Cook K.H., 1995, AJ 110, 192
Arimoto N., Sofue Y., Tsujimoto T., 1996, PASJ 48, 275
Binggeli B., 1994, in "Panchtomatic view of galaxies - their evolutionary puzzle", Eds. G.Hensler, Ch.Theis, J.Gallagher (Editions Frontieres), p.173
Brouillet N., Baudry A., Combes F., 1988, A&A 196, L17
Brouillet N., Baudry A., Combes F., Kaufman M., Bash F., 1991, A&A 242, 35
Cardelli J.A., Clayton G.C., Mathis J.S., 1989, ApJ 345, 245
Carignan C., 1985, ApJSS 58, 107
Carignan C., Puche D., 1990, AJ 100, 394
Combes F., Encrenaz P.J., Lucas R., Weliachew L., 1978, A&A 67, L13
de Vaucouleurs G., 1958, ApJ 128, 465
de Vaucouleurs G., 1959, ApJ 130, 728
de Vaucouleurs G., 1963, ApJ 137, 720
de Vaucouleurs G., Davoust E., 1980, ApJ 239, 783
de Vaucouleurs G., de Vaucouleurs A., Corvin H.G., Buta R.J., Paturel J., Fouque P., 1991, Third Reference Catalog of bright Galaxies (New York: Springer) (RC3)
Dopita M.A., Evans I.N., 1986, ApJ 307, 431
Edmunds M.G., Pagel B.E.J., 1984, MNRAS 211, 507
Ferrarese L., Freedman W.L., Hill R.J., et al, 1996a, ApJ 464, 568
Ferrarese L., Livio M., Freedman W.L., et al, 1996b, ApJ 468, L95
Ferrini F., Galli D., 1988, A&A 195, 27
Ferrini F., Matteucci F., Pardi C., Penco U., 1992, ApJ 387, 138
Freedman W.L., Wilson C.D., Madore B.F., 1991, ApJ 372, 455
Garnett D.R., Shields G.A., Skillman E.D., Sagan S.P., Dufour R.J., 1997, ApJ
Harnett J.I., Wielebinski R., Bajaja E., Reuter H.-P., Hummel E., 1991, Proc. ASA 9, 258
Hoessel J.G., Melnick J., 1980, A&A 84, 317
Israel F.P., Tacconi L.J., Baas F., 1995, A&A 295, 599
Kamphuis J., Sancisi R., 1994, in "Panchtomatic view of galaxies - their evolutionary puzzle", Eds. G.Hensler, Ch.Theis, J.Gallagher (Editions Frontieres), p.317
Kenney J.D., Scoville N.Z., Wilson C.D., 1991, ApJ 366, 432
Kenney J.D., Young J.S., 1988, ApJSS 66, 261
Kennicutt R.C., Garnett D.R., 1996, ApJ 456, 504
Knapen J.H., Beckman J.E., 1996, MNRAS 283, 251
Knapen J.H., Beckman J.E., Cepa J., Nakai N., 1996, A&A 308, 27
Koper E., Dame T.M., Israel F.P., Thaddeus P., 1991, ApJ 383, L11
Lee M.G., Freedman W.L., Madore B.F., 1993, Apj 417, 553
Lequeux J., 1996, in "The interplay between massive star formation, the ISM and galaxy evolution", Eds. Kunth D., Guiderdoni B., Heydari-Malayeri M., Thuan T.X. (Editions Frontieres), p.105.
Maeder A. 1992, A&A 264, 105
Matteucci F., François P., 1989, MNRAS 239, 885
McCall M.L., Rybski P.M., Shields G.A., 1985, ApJSS 57, 1
Molla M., Ferrini F., Diaz A.I., 1996, ApJ 466, 668
Molla M., Ferrini F., Diaz A.I., 1997, ApJ 475, 519
Newton K., 1980, MNRAS 190, 689
Okamura S., Takase B., Kodaira K., 1997, PASJ 29, 567
Pagel B.E.J., Tautvaisiene G., 1995, MNRAS 276, 505
Pardi C., Ferrini F., 1994, ApJ 421, 491
Pilyugin L.S., 1996, A&A 310, 751
Pilyugin L.S., Edmunds M.G., 1996, A&A 313, 792
Renzini A., Voli M., 1981, A&A 94, 175
Rots A.H., 1975, A&A 45, 43
Ryder S.D., Staveley-Smith L., Malin D., Walsh W., 1995, AJ 109, 1592
Sage L.J., Westpfahl D.J., 1991, A&A 242, 371
Salpeter E.E., 1955, ApJ 121, 161
Sandage A., 1986, A&A 161, 89
Schmidt B.P., Kirshner R.P., Eastman R.G., et al, 1994, ApJ 432, 42
Schweizer F., 1976, ApJSS 31, 313
Sharina M.E., Karachentsev I.D., Tikhonov N.A., 1996, A&ASS 119, 499
Shostak G.S., van der Kruit P.C., 1984, A&A 132, 20
Skillman E.D., Kennicutt R.C., Shields G.A., Zaritsky D., 1996, ApJ 462, 147
Tacconi L.J., Young J.S., 1986, ApJ 308, 600

Talbot R.J., Jensen E.B., Dufour R.J., 1979, ApJ 229, 91
Tantalo R., Chiosi C., Bressan A., Fagotto F., 1996, A&A 311, 361
Thomasson M., Donner K.J., 1993, A&A 272, 153
Thornley M.D., Wilson C.D., 1995, ApJ 447, 616
Tilanus R.P.J., Allen R.J., 1993, A&A 274, 707
Tosi M., 1988a, A&A 197, 33
Tosi M., 1988b, A&A 197, 47
van der Hulst J.M., 1979, A&A 75, 97
Vila-Costas M.B., Edmunds M.G., 1992, MNRAS 259, 121
Walsh J.R., Roy J.-R., 1997, Preprint ESO No 1219
Walterbos R.A.M., Kennicutt R.C., 1988, A&A 198, 61
Warmels R.H., 1988, ApJSS 72, 427
Watanabe M., 1983, Annals of the Tokyo astronomical observatory, second series v. XIX, 121
Wevers B.M.H.R., van der Kruit P.C., Allen R.J., 1986, A&ASS 66, 505
Whitmore B.C., Kirshner R.P., 1982, AJ 87, 500
Wilson C.D., 1995, ApJ 448, L97
Zaritsky D., Kennicutt R.C., Jr., Huchra J.P., 1994, ApJ 420, 87 (ZKH)